CRYSTAL GROWTH & DESIGN

Article

Cite This: Cryst. Growth Des. XXXX, XXX, XXX−XXX

pubs.acs.org/crystal

Solid State Selection between Nearly Isoenergetic Tautomeric Forms Driven by Right Hydrogen-Bonding Pairing

Sandra Fusco,*[,†] Emmanuele Parisi,[†] Antonio Carella,[†] Amedeo Capobianco,*[,‡] Andrea Peluso,[‡] Carla Manfredi,[†] Fabio Borbone,[†] and Roberto Centore*[,†]

[†]Department of Chemical Sciences, University of Naples Federico II, Via Cintia, I-80126 Naples, Italy

[‡]Department of Chemistry and Biology, University of Salerno, Via Giovanni Paolo II, 132, I-84084 Fisciano, Salerno, Italy

Supporting Information

ABSTRACT: We have prepared new hydroxyphenyl derivatives of [1,2,4]triazolo[3,2-*c*][1,2,4]triazole and investigated their tautomeric behavior, for the neutral and the monoprotonated forms, either computationally and experimentally in solution and the solid state. The results of our analysis indicate that the tautomeric behavior, in particular for the monoprotonated forms, is strongly dependent on the position of the OH group in the phenyl ring. The different position of the group (ortho, meta, para) has an effect on the relative energy of the various tautomeric forms of the cations but also on their ability to get an optimum packing, which is driven by directional hydrogen bonds. In particular, with the OH in para position, the two tautomers 1*H*-3*H* and 2*H*-3*H* of the singly protonated form have a similar energy and can be selectively isolated in the solid state with different counterions; with OH in the meta position, though the energy difference between the tautomers is even smaller, only the 2*H*-3*H* is present in the solid state, because of optimum packing interactions (hydrogen-bonding pairing); finally, with ortho OH, only the 1*H*-3*H* is isolated in the solid state because it has energy significantly lower than 2*H*-3*H*.

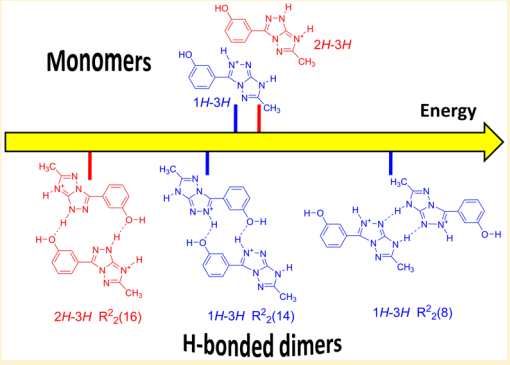

INTRODUCTION

Tautomers are structural isomers in ready equilibrium between each other.[1] In the most common case of tautomerism, i.e., prototropism, tautomers differ in the position of a hydrogen atom inside the molecule and in the distribution of π electrons.

A remarkable example of the importance of tautomers in chemistry is provided by the landmark second paper of Watson and Crick on the structure of DNA.[2] In that paper, the authors proposed the hydrogen-bonding pairing scheme between purine and pyrimidine bases, which is rooted in the most probable tautomeric forms of the bases. They also raised the hypothesis that less probable (i.e., noncanonical) tautomeric forms of the bases could lead to wrong pairings and so to mutations (see Supporting Information). This "rare tautomer" hypothesis for spontaneous mutagenesis has been confirmed over the years.[3,4]

In a certain sense, tautomers can be considered as "living molecules",[5] because of the thermodynamic equilibrium they undergo. In fact, the relative amounts of the different forms can be altered by physical or chemical factors[6−10] (temperature, solvent, pH, mechanochemical processes, etc.), and so a tautomeric system can face a change in ambient conditions by favoring one form over the others. This responsiveness of tautomeric systems is potentially appealing for the development of smart materials and single-molecule-based devices.[11,12]

The dynamic equilibrium between the different tautomeric forms of a compound in solution can lead, in principle, to different outcomes for the crystallization from solution: crystallization of only one tautomeric form (likely, but not necessarily, the most stable in solution), cocrystallization of different tautomers in the same lattice, concomitant formation of crystals of different tautomeric forms. A recent detailed analysis has shown that crystallization of different tautomers of the same compound is a rather rare occurrence.[13] In particular, only about 0.5% of molecules able to tautomerize and archived in the Cambridge Structural Database CSD[14] are actually observed in different tautomeric forms in the solid state. This can be related, at least in part, to the fact that for many potentially tautomeric systems, the energy difference between the tautomers is rather high (>3 kcal/mol), and so only one form is prevailing by far in solution and found in the crystals. However, there are counterexamples to this simple explanation, i.e., tautomeric couples with a higher energy difference that are isolated in the solid state. At any rate, a reasonable condition for the observation of different tautomers in the solid state is to reduce their molecular energy difference, a target that can be achieved by introducing suitable substituent groups within the compound.

In the realm of fused-ring heteroaromatic systems that we have studied over the years,[15−17] we have found in the

Received: July 31, 2018
Revised: September 8, 2018
Published: September 11, 2018

DOI: 10.1021/acs.cgd.8b01158
Cryst. Growth Des. XXXX, XXX, XXX−XXX

[1,2,4]triazolo[3,2-*c*][1,2,4]triazole, Chart 1, a heterocyclic system with a rich tautomeric behavior.[18−20]

Chart 1. Neutral and Singly Protonated Triazolotriazoles[a]

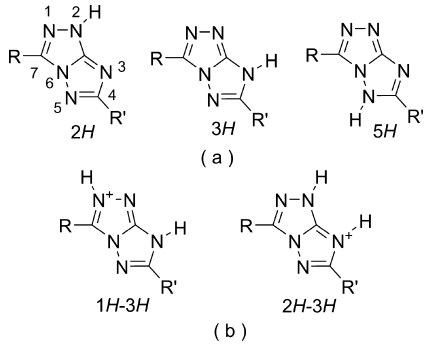

[a](a) The three canonical tautomeric forms of neutral [1,2,4]triazolo-[3,2-*c*][1,2,4]triazole, with atom numbering shown for the 2*H* tautomer. (b) The two lowest energy tautomers of monoprotonated [1,2,4]triazolo[3,2-*c*][1,2,4]triazole (only one resonance form is shown).

We have found that the relative energy of the three tautomers of the neutral molecule, Chart 1a, and of the two most stable tautomers of the monoprotonated species, Chart 1b, can be significantly modulated by acting on the substituents, mostly in position 7, and on the polarity of the solvent. For the neutral compounds, in all the cases investigated, the energy trend of the tautomers is $E(2H) < E(3H) \ll E(5H)$; in particular, the energy of the 5*H* tautomer is always prohibitive (+10.8 kcal/mol with respect to 2*H* in the most favorable case),[18] while, for the 3*H* tautomer, with R = *p*-nitrophenyl and R′ = methyl, an energy difference of +0.9 kcal/mol with respect to 2*H* has been calculated in water.[18] For the monoprotonated species, Chart 1b, the pattern is more intriguing. In fact, the energy difference between the two tautomers is small (1.9 kcal/mol in the worst case);[20] moreover, electron withdrawing groups in position 7 make the tautomer 1*H*-3*H* more stable, while with electron donor groups the tautomer 2*H*-3*H* is more stable.[19] In the case of the compound with R = 4-hydroxyphenyl and R′ = methyl, TT5 of ref 20, the energy difference between the two tautomers is only 0.6 kcal/mol (1*H*-3*H* more stable) so they are present in a comparable amount in solution and were selectively precipitated by using different counterions (chloride for 1*H*-3*H* and sulfate for 2*H*-3*H*).[20]

In the present paper we further extend the study of the tautomeric behavior of derivatives of [1,2,4]triazolo[3,2-*c*][1,2,4]triazole, by considering the two structural isomers of TT5 in which the hydroxy group is in the meta (TT6) and ortho (TT7) position, Chart 2.

Chart 2. Chemical Diagrams of the Studied Compounds (Only 2*H* Tautomer Shown)

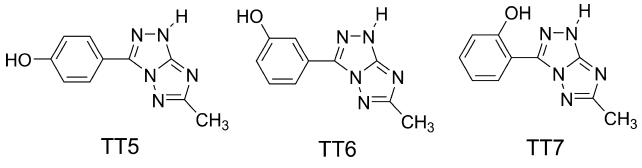

RESULTS AND DISCUSSION

Computational and Experimental Analysis in Solution. We have performed a preliminary computational analysis of the energy of the tautomers of TT6 and TT7 in the neutral and monoprotonated forms, to be compared with the results for TT5 that we have already published.[20] While for TT5 a single conformer was found for the neutral and monoprotonated species, in the case of TT6 and TT7 four different conformers were found, differing for the orientation of the hydroxy-phenyl ring and of the methyl group. The conformers are indicated by a three-letter symbol, where each letter can be *c* or *t* (e.g., *tcc*). The explanation of the symbol is given in Chart 3 below.

Chart 3. Definition of the Conformers for TT6 and TT7

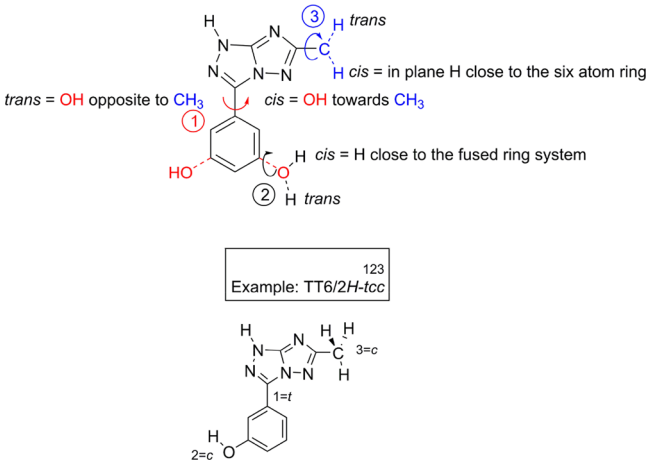

Neutral Molecules. The relative energies of tautomers (2*H*, 3*H*, 5*H*) of neutral TT6 follow a quite similar trend to TT5, see Table 1: 2*H* is the most stable, both in the gas phase and in polar medium; 3*H* is significantly stabilized in polar medium, but its energy, as compared to 2*H*, is still high (2.7 kcal/mol) in order that it be found in appreciable amount.

Table 1. Computed Relative Energies (kcal/mol), in Reference to 2*H*, of Tautomers 3*H* and 5*H* of Neutral TT6, TT7, and TT5[a]

	gas		water	
	3*H*	5*H*	3*H*	5*H*
TT5[b]	9.5	23.0	3.2	13.9
TT6[c]	8.8 (8.2)	21.8 (21.1)	2.7 (2.7)	13.4 (12.9)
TT7[c]	6.2 (6.0)	19.3 (18.7)	1.0 (0.9)	12.1 (11.8)

[a]Zero point vibration energy (ZPVE) corrected values are reported in parentheses. [b]Data for TT5 are taken from ref 20. [c]The energy of the most stable conformer of each tautomer is reported.

On the other hand, for neutral TT7 the 3*H* tautomer, in polar medium, is less stable than 2*H* by 1.0 kcal/mol only.

In Table 2 are reported the computed energies of the different conformers of tautomers 2*H* of neutral TT6 and TT7 (data for conformers of TT7/3*H* are reported in Supporting Information). It should be noted that the full counting of the conformers gives eight outcomes ($2^3 = 8$). However, we have found that the conformation of the methyl group is always *c*, both for TT6 and TT7. In fact, even starting from methyl in conformation *t*, the density functional theory (DFT) geometry

DOI: 10.1021/acs.cgd.8b01158
Cryst. Growth Des. XXXX, XXX, XXX−XXX

Table 2. Predicted Relative Energies (kcal/mol) of the Possible Conformers of TT6/2*H* and TT7/2*H*[a]

	TT6/2*H* gas	TT6/2*H* water	TT7/2*H* gas	TT7/2*H* water
	E_{el}	E_{el}	E_{el}	E_{el}
ccc	**0.0 (0.0)**	**0.0 (0.0)**	2.5 (2.4)	2.6 (2.2)
ctc	0.8 (0.7)	0.0 (0.1)	9.3 (8.8)	5.4 (5.0)
tcc	0.3 (0.3)	0.0 (0.2)	**0.0 (0.0)**	**0.0 (0.0)**
ttc	0.7 (0.6)	0.0 (0.2)	8.4 (8.0)	5.3 (5.0)

[a]Zero point vibration energy (ZPVE) corrected values are reported in parentheses. The most stable conformation is highlighted in bold.

optimization changes its conformation in *c*. Therefore, only four possible conformers are predicted by computations.

Both in the gas phase and in water, the four conformers of TT6/2*H* are almost isoenergetic. Instead, in the case of TT7/2*H* (and TT7/3*H*, see Supporting Information) the two conformers that allow the formation of the intramolecular hydrogen bond with the ortho OH are by far more stable. In particular, the conformer *tcc*, in which the intramolecular hydrogen bond involves N1 as the acceptor, is predicted to be more stable than *ccc*, in which N5 is the acceptor, by about 2.5 kcal/mol, as shown in Chart 4.

Chart 4. Two Conformers of TT7/2*H* That Allow the Formation of the Intramolecular Hydrogen Bond

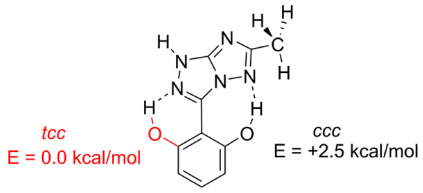

TT7/2*H*

Of course, the conformational analysis that we have performed is only applicable to dilute solutions, because the possible formation of dimers or *n*-mers with intermolecular hydrogen bonds has not been considered.

Singly Protonated TT6 and TT7. Calculations for singly protonated TT6 and TT7 have been performed in water. Out of the possible six tautomers of singly protonated species, tautomers 1*H*-3*H* and 2*H*-3*H*, see Chart 1b, are expected to be the most stable, on the basis of our previous studies.[19,20] The tautomer 1*H*-2*H* has been tested for comparison.

Singly protonated TT6 and TT7 have several populated conformers. For data of Table 3 the energy of the most stable conformer for each tautomer has been considered.

In the case of TT6, singly protonated 1*H*-3*H* and 2*H*-3*H* tautomers are predicted almost isoenergetic in solution, and for both four conformers are populated (Table 4).

Table 3. Computed Relative Energy (kcal/mol, not Including ZPVE) of the Most Relevant Tautomers of Singly Protonated TT5, TT6, and TT7 in Water

	TT5[a]	TT6	TT7
1*H*-2*H*	13.8	14.6	13.6
1*H*-3*H*	0.0	0.0	0.0
2*H*-3*H*	0.6	0.2	2.5

[a]Data for TT5 are taken from ref 20.

Table 4. Predicted Relative Energies (kcal/mol) of the Conformers of the Most Significant Tautomers of Protonated TT6 and TT7 in Water[a]

	TT6/1*H*-3*H*	TT6/2*H*-3*H*	TT7/1*H*-3*H*	TT7/2*H*-3*H*
	E_{el}	E_{el}	E_{el}	E_{el}
ccc	0.1 (0.0)	0.1 (0.3)	5.3 (5.0)	3.8 (3.5)
ctc	**0.0 (0.0)**	0.0 (0.1)	4.8 (4.5)	3.3 (2.9)
tcc	0.3 (0.4)	0.0 (0.1)	goes to *ttc*	**0.0 (0.0)**
ttc	0.1 (0.1)	**0.0 (0.0)**	**0.0 (0.0)**	3.6 (3.4)

[a]Zero point vibration energy (ZPVE) corrected values are reported in parentheses. The most stable conformation is highlighted in bold.

For singly protonated TT7, on the other hand, the tautomer 1*H*-3*H* is predicted to be far more stable than the others, and for this tautomer, only one conformer is populated: *ttc* (Chart 5). Remarkably, in this tautomer, the intramolecular hydrogen

Chart 5. Two Conformers of TT7[1*H*-3*H*]$^+$[a]

TT7[1*H*-3*H*]$^+$

[a]Only one resonance form is shown.

bond between OH donor and N1 acceptor of the neutral molecule (Chart 4) is no longer present, because the H atom bonded to O is on the opposite side; there is, instead, an intramolecular hydrogen bond between N−H donor and OH acceptor, Chart 5.

For protonated TT7[1*H*-3*H*]$^+$, a further conformation with an O−H···N intramolecular hydrogen bond could be devised, in which N5 would be the acceptor (conformer *ccc* of Table 4, see also Chart 5). However, that conformation turns to be energetically disfavored because, according to computations, the positive charge of the molecule-ion would be mostly localized on N6 (Chart 5).

Neutral TT6 and TT7 (H_2L) can accept a proton, forming the cationic species H_3L^+, and can release up to two protons, forming the species HL^- and L^{2-}. In particular, the most acidic hydrogen atom of the neutral molecules is N−H, and, therefore, in the monoanionic HL^- species, the phenolic O−H hydrogen is retained.[20] The acid−base equilibria in solution have been studied at 25 °C by potentiometric-spectrophotometric titrations in constant ionic medium NaCl 0.5 M/ethanol 4% (v/v). UV−vis absorption spectra of TT6 recorded at different pH and constant total concentration of TT6 are reported in Figure 1a, and they show a remarkable dependence on pH. In Figure 1b are reported the correspondent absorbance vs pH data at four different wavelengths (similar data for TT7 are reported in Supporting Information).

The calculated conditional equilibrium constants are reported in Table 5.

The most remarkable difference in the data of Table 5 is in the pK_{a3} values of TT5 and TT7, which differ by about 2 units. This can be an electrostatic effect related to the space separation between the negative charges of the dianion L^{2-},

DOI: 10.1021/acs.cgd.8b01158
Cryst. Growth Des. XXXX, XXX, XXX−XXX

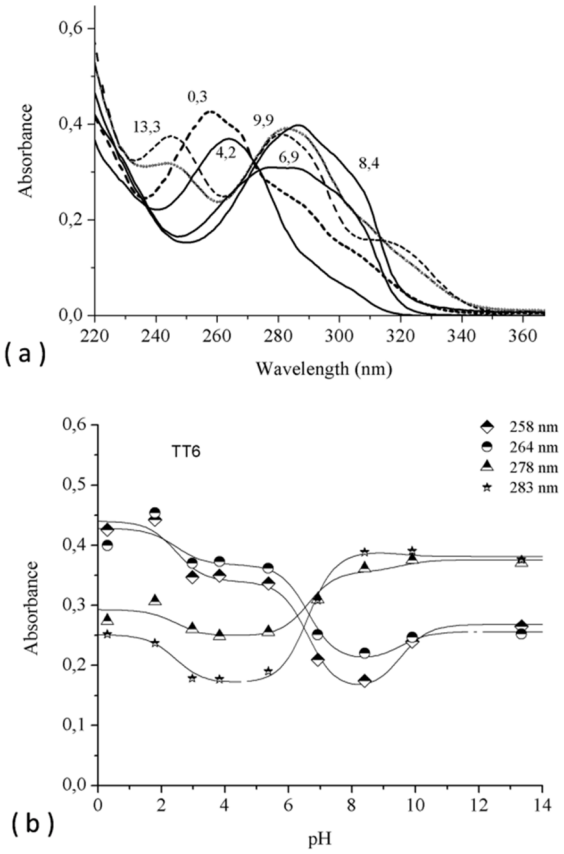

Figure 1. (a): UV−vis absorption spectra of TT6 at constant total concentration, $c_M = 3.5 \times 10^{-5}$ M, in NaCl 0.5 M/ethanol 4% (v/v) recorded at $0.3 \leq pH \leq 14$; (b) absorbance/pH data, at four different wavelengths, taken from panel a; the continuous curves were obtained by fitting the experimental points using the Bouger−Lambert−Beer equation (see Supporting Information).

Table 5. Acid−Base Reactions and Equilibrium Constants (in NaCl 0.5 M/ethanol 4%, with Estimated Standard Deviations in Parentheses) at 25 °C for TT5, TT6, and TT7

reaction	TT5[a]	TT6	TT7
$H_3L^+ + H_2O = H_2L + H_3O^+$	pK_{a1} = 2.02(5)	pK_{a1} = 2.45(3)	pK_{a1} = 2.21(2)
$H_2L + H_2O = HL^- + H_3O^+$	pK_{a2} = 6.97(5)	pK_{a2} = 6.62(4)	pK_{a2} = 6.55(3)
$HL^- + H_2O = L^{2-} + H_3O^+$	pK_{a3} = 9.00(5)	pK_{a3} = 9.67(7)	pK_{a3} = 10.98(6)

[a]Data for TT5 are taken from ref 20.

that, for TT7, is considerably reduced, this possibly leading to a diminution of the acid strength of HL^-.

The behavior of TT*n* compounds in solution is complex. Indeed, the final composition of the solution results from three acid base reactions involving four different species and regulated by relatively close values of pK_a, as indicated by the distribution diagram of TT6 reported in Figure 2.

Things are further complicated by tautomeric equilibria affecting the singly protonated species. As an example, at pH = 2.45 and T = 298 K, TT6 exists as a 50% mixture of the neutral and monoprotonated forms; the monoprotonated form, in turn, is predicted to be an equilibrium mixture of the 1*H*-3*H* (~60%) and 2*H*-3*H* (~40%) tautomers (see Figure S22 in Supporting Information).

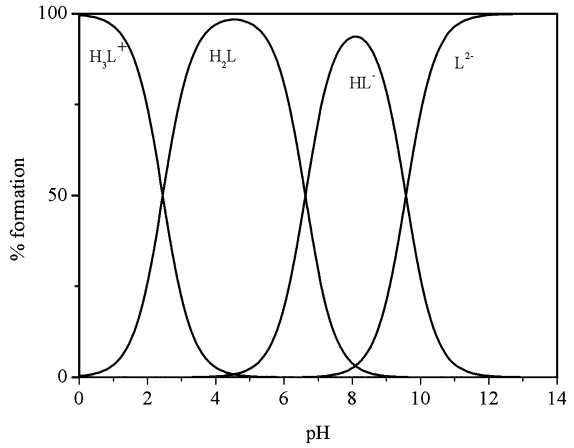

Figure 2. Distribution diagram of TT6, drawn using the equilibrium constants of Table 5.

Crystallographic Analysis. The crystallographic analysis has been performed on the singly protonated forms H_3L^+ of TT6 and TT7, that will be indicated as $TT6H^+$ and $TT7H^+$. As we have shown above, the computational analysis suggests that for $TT6H^+$ the two most stable tautomers, i.e., 1*H*-3*H* and 2*H*-3*H*, are almost isoenergetic, and so, both being present in solution, in principle both could be isolated in the crystals. For TT7, on the other hand, only the 1*H*-3*H* is predicted to be populated in solution and should be found in the crystals. In order to assess the propensity of the different tautomers to crystallize, in particular for TT6 for which computations suggest nearly isoenergetic structures, we have prepared several salts of the monocations, using different anions, both monatomic (chloride, bromide) and molecular (perchlorate, hydrogensulfate, sulfate).

The results for $TT6H^+$ are shown in the Ortep diagrams of Figures 3, 4, 5, 6, and 7.

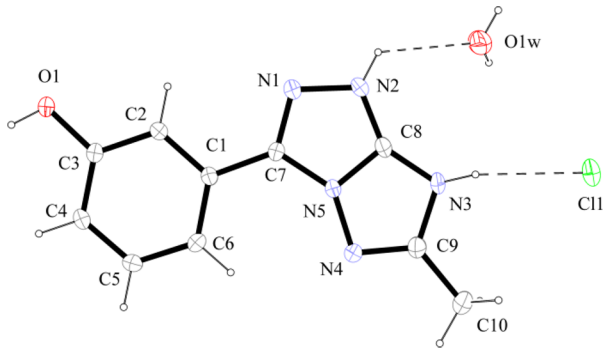

Figure 3. Ortep diagram of TT6·HCl·H_2O. Thermal ellipsoids are drawn at the 30% probability level. Selected hydrogen bonds are indicated by dashed lines.

In all the cases, the 2*H*-3*H* tautomer is observed, in the conformation *ttc*. The selective crystallization of this tautomer seems independent of the anion (monatomic, molecular, mononegative, dinegative) and of the presence of water molecules in the lattice, so it cannot be happenstance. Completely different results were obtained for TT5. In that case, the two tautomers 1*H*-3*H* and 2*H*-3*H*, predicted to differ in energy by 0.9 kcal/mol by DFT computations, were selectively precipitated, respectively, as chloride and sulfate.[20] We think that the persistent selection of the 2*H*-3*H* tautomer

DOI: 10.1021/acs.cgd.8b01158
Cryst. Growth Des. XXXX, XXX, XXX−XXX

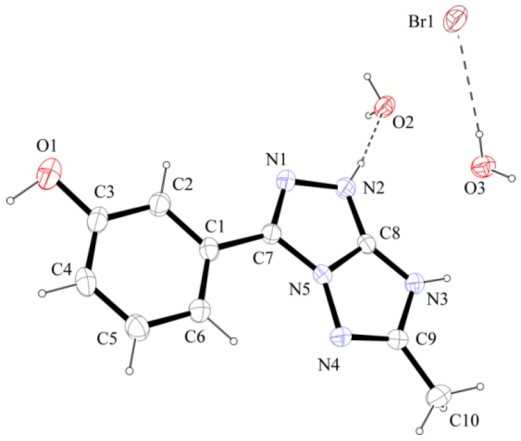

Figure 4. Ortep diagram of TT6·HBr·2H_2O. Thermal ellipsoids are drawn at the 30% probability level. Selected hydrogen bonds are indicated by dashed lines.

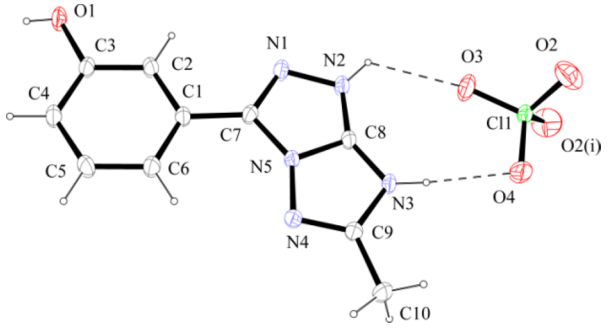

Figure 5. Ortep diagram of TT6·$HClO_4$. Thermal ellipsoids are drawn at the 30% probability level. Selected hydrogen bonds are indicated by dashed lines.

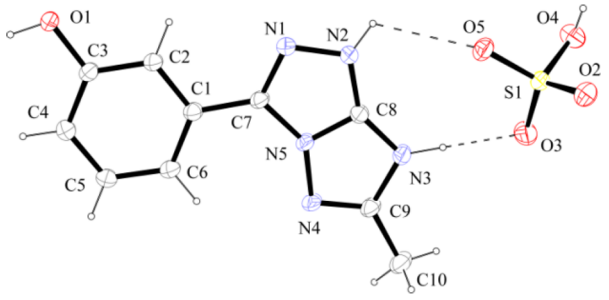

Figure 6. Ortep diagram of (TT6H)(HSO_4). Thermal ellipsoids are drawn at the 30% probability level. Selected hydrogen bonds are indicated by dashed lines.

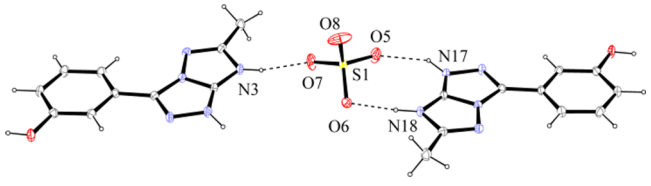

Figure 7. Partial Ortep diagram of 2[(TT6H)(HSO_4)]·(TT6H)$_2SO_4$·4H_2O, in which only the sulfate ion and the two cation molecules hydrogen-bonded to it are shown. Thermal ellipsoids are drawn at the 30% probability level. Only selected atoms are numbered for clarity. Selected hydrogen bonds are indicated by dashed lines.

in crystals of TT6 is related with a better pairing of cation molecules through hydrogen bonding, as compared with the 1*H*-3*H* tautomer. This is illustrated in Chart 6, showing that the formation of H-bonded dimers through symmetry operations allowed in common space groups, for instance, crystallographic inversion centers or binary rotation axes, is accomplished through optimum hydrogen-bonding geometry only in the case of the 2*H*-3*H* tautomer. In fact the two possible dimers corresponding to 1*H*-3*H* tautomer (see Chart 6) are penalized by the lower acceptor capability of N2 atom in the case of $R_2^2(8)$ and by the geometry, in the case of dimer $R_2^2(14)$.

Actually, the $R_2^2(16)$ dimer of Chart 6 is present in all the structures investigated of $TT6H^+$ salts, with the only exception of the bromide salt, so in four structures out of five (80%), Figure 8 (see also Supporting Information for full packing diagrams); moreover, if we consider that in some crystal structures the independent unit contains more than one cation, the $R_2^2(16)$ dimer is observed in seven cases out of eight (88%). This suggests it is a highly robust synthon.[21]

These arguments have been checked by energy calculations on the dimers. In Table 6 are reported the interaction energies of the dimers, E_{int}, defined as $E_{int} = E(A_2) - 2E(A)$, where $E(A_2)$ is the energy of the optimized dimer A_2 and $E(A)$ is the energy of the optimized monomer A.

Interaction energies are positive because the DFT optimization of the dimers has been performed without counterions, and so there is repulsion between the two cations forming the dimer. However, the occurrence of zero first derivatives for the nuclear configurations corresponding to the optimized dimers and the concomitant occurrence of real and positive vibrational frequencies indicate that the optimized dimers do correspond to minima of energy. Of course they are relative minima of the hypersurface of the potential energy $V(x_1,y_1,z_1, \cdots, x_N,y_N,z_N)$ [x_i are the nuclear coordinates].

That said, the results of Table 6, that have been obtained without imposing any constraint during the optimization, indicate that for the dimer 2*H*-3*H* $R_2^2(16)$ the repulsion is considerably lower than 1*H*-3*H* $R_2^2(14)$ (by about 6 kcal/mol) and lower by far than 1*H*-3*H* $R_2^2(8)$ (by about 14 kcal/mol). If we consider that the difference in latttice energy of polymorphs is generally within 1−2 kcal/mol,[22] we can exclude that tautomer 1*H*-3*H* of TT6, though having energy 0.2 kcal/mol lower than 2*H*-3*H* (see Table 3), be found in crystals, and this because of packing interactions (H bonding pairing). Moreover, the analysis of the geometry of the optimized dimers (see Figures S13−S15 in Supporting Information) shows that in the case of 2*H*-3*H* $R_2^2(16)$ the dimer has C_{2h} symmetry, as basically found in the crystals. In the other two cases, repulsions between nonbonded hydrogen atoms of the two monomers induce a nonplanar geometry of the dimer that only retains C_i symmetry. All the above arguments could also suggest that the 2*H*-3*H* $R_2^2(16)$ dimers are already present in concentrated solutions of the salts[23,24] and that crystallization of salts of the $TT6H^+$ cation can be actually regarded as crystallization of the dimers.

Ortep diagrams of the crystal structures of salts of TT7 (chloride, bromide, and perchlorate) are reported in Figures 9, 10, and 11. In all the cases the 1*H*-3*H* tautomer is present, as expected on the basis of the energy computations. Interestingly, the conformation of the cation detected in all crystals is always *ttc*, in line with theoretical results, finding *ttc* more

DOI: 10.1021/acs.cgd.8b01158
Cryst. Growth Des. XXXX, XXX, XXX−XXX

Chart 6. Possible Pairing of $TT6H^+$ Cations (*ttc* Conformer) through Hydrogen Bonds in Tautomers 2*H*-3*H* and 1*H*-3*H*

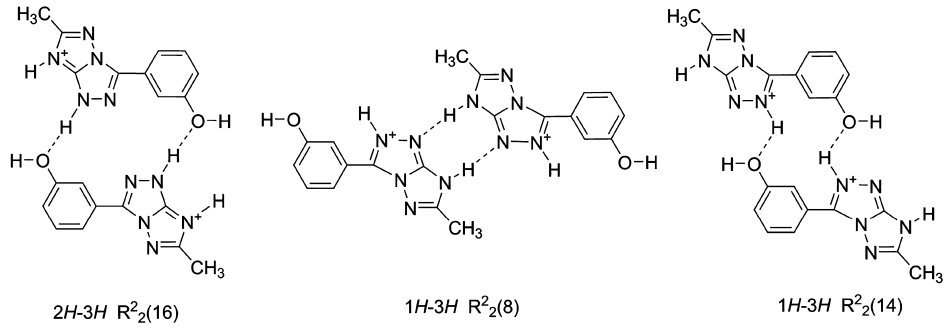

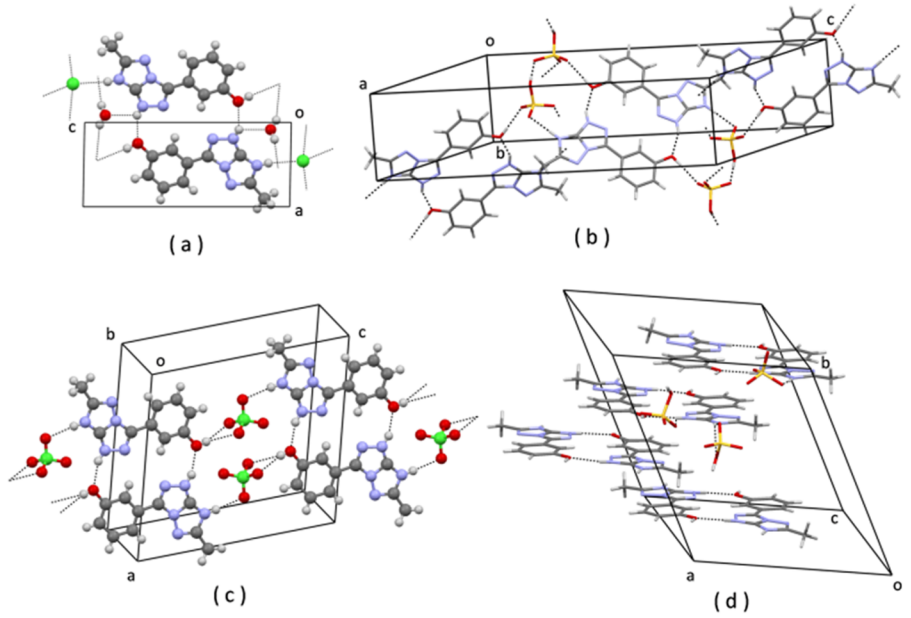

Figure 8. Partial packing diagrams of some salts of the $TT6H^+$ cation. (a) $TT6{\cdot}HCl{\cdot}H_2O$; (b) $(TT6H)(HSO_4)$; (c) $TT6{\cdot}HClO_4$; (d) $2[(TT6H)(HSO_4)]{\cdot}(TT6H)_2SO_4{\cdot}4H_2O$. In some cases, water molecules are not shown for clarity. Selected hydrogen bonds are indicated by dashed lines.

Table 6. Interaction Energies of Dimers of Chart 6, in kcal/mol

dimer	E_{int}
2*H*-3*H* $R_2^2(16)$	18.0
1*H*-3*H* $R_2^2(8)$	32.3
1*H*-3*H* $R_2^2(14)$	23.8

stable by ≈5 kcal/mol than the other conformations (see Table 4).

In particular, it is confirmed that the intramolecular hydrogen bond between O−H donor and N1 acceptor, present in the neutral molecule, is no longer present in the protonated 1*H*-3*H* tautomer. This features a formal conformational switching of the OH hydrogen upon protonation, simultaneous to the tautomeric 2*H* → 1*H*-3*H* switching, as shown in Scheme 1.

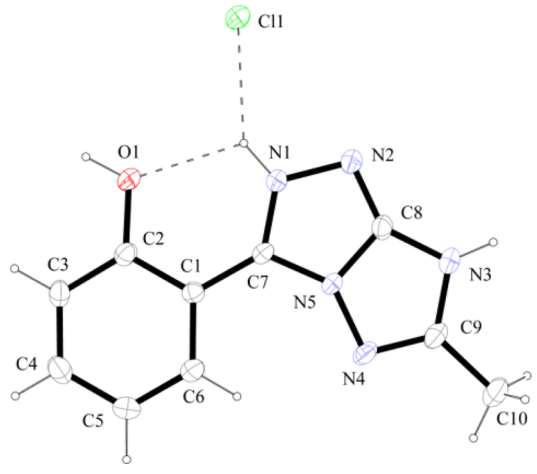

Figure 9. Ortep diagram of TT7·HCl. Thermal ellipsoids are drawn at the 30% probability level. Selected hydrogen bonds are indicated by dashed lines.

EXPERIMENTAL SECTION

Materials and Methods. All reagents were analytical grade and were used without further purification. Melting points were determined by temperature controlled optical microscopy (Zeiss Axioskop polarizing microscope equipped with a Mettler FP90 heating stage). NMR spectra were recorded with Bruker or Varian spectrometers operating at 400 MHz, in $CDCl_3$ or DMSO-d_6. ESI mass spectrometric analyses were recorded with an Applied Biosystems API 2000 mass spectrometer equipped with an electrospray source used in the positive mode.

DOI: 10.1021/acs.cgd.8b01158
Cryst. Growth Des. XXXX, XXX, XXX−XXX

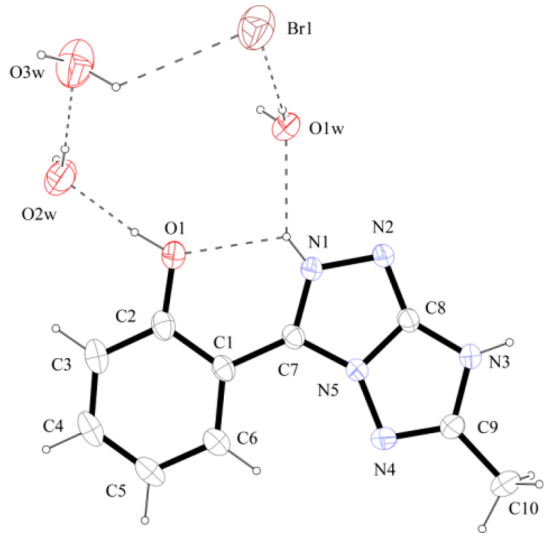

Figure 10. Ortep diagram of TT7·HBr·3H_2O. Thermal ellipsoids are drawn at the 30% probability level. Selected hydrogen bonds are indicated by dashed lines.

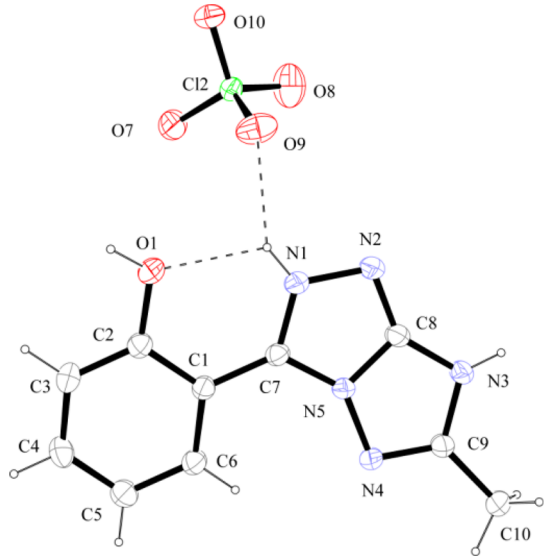

Figure 11. Ortep diagram of TT7·$HClO_4$. Thermal ellipsoids are drawn at the 30% probability level. Selected hydrogen bonds are indicated by dashed lines. Only half of the crystallographic independent unit is shown. The solvent water molecule is not shown.

Scheme 1. Formal Conformational and Tautomeric Switching of TT7 upon Protonation

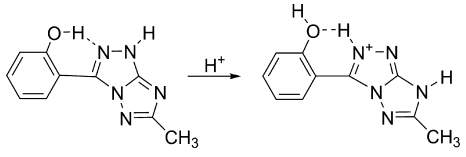

General Synthetic Procedures. The synthesis of TT6 and TT7 was performed according to the procedure already described by us,[20] and that is shortly outlined here (full details are given in Supporting Information). Starting from 3-hydroxybenzoic acid (for TT6) or salicylic acid (for TT7), reaction with diaminoguanidine monohydrochloride in polyphosphoric acid (PPA), at 150 °C overnight, affords 5-(3-hydroxyphenyl)-3,4-diamino-1,2,4-triazole and 5-(2-hydroxyphenyl)-3,4-diamino-1,2,4-triazole, respectively.[25] Reaction of the diaminotriazole with acetic anhydride at reflux gives the diacetylated triazolo-triazole that, after basic hydrolysis and acid recovery, affords pure TT6 and TT7. Single crystals of salts of monoprotonated TT6 and TT7 cations were prepared by slow evaporation of solutions obtained by solving 10 mg of the neutral compound in 20 mL of 1 M solutions of the inorganic acid (HCl, HBr, $HClO_4$, H_2SO_4).

Acid−Base Equilibria. The protolytic equilibria of TT6 and TT7 were studied by UV−vis absorption spectroscopy in 0.5 M NaCl−4% ethanol (v/v), as the ionic medium, following the same procedure described in ref 20. The experiments were performed as acid−base titrations at constant total concentration of TT6/TT7 without varying the 0.5 M concentration of Cl^-. The investigated pH range extends from 0.3 to 14. For each experimental point, the equilibrium free proton concentration was evaluated from the measured electromotive force at the ends of the galvanic cell GE/TS/RE, where TS indicates the test solution, GE is the glass electrode, and RE is a reference electrode (0.5 M NaCl|Hg_2Cl_2|Hg(Pt)) placed outside but electrically connected to TS through a salt bridge. All the experiments were carried out in air in a thermostat, at 25.00 ± 0.03 °C. Potentiometric experimental data were collected by means of an automatic data acquisition system based on Hewlett-Packard (HP) instrumentation. Coulometric variations of the solution composition were carried out using a Hewlett-Packard "DC Power Supply". Absorption spectra were recorded with a Varian Cary 50 UV−vis spectrophotometer using 1 cm cell. The primary spectrophotometric data (A, pH, λ) were numerically analyzed by the computerized program HYPERQUAD.[26] A detailed description of the mathematical procedures is given in Supporting Information.

Crystallography. All data for crystal structure determinations were measured on a Bruker-Nonius KappaCCD diffractometer equipped with Oxford Cryostream 700 apparatus, using graphite monochromated MoKα radiation (λ = 0.71073 Å). Reduction of data and semiempirical absorption correction were done using SADABS program.[27] The structures were solved by direct methods (SIR97 program[28]) and refined by the full-matrix least-squares method on F^2 using SHELXL-2016/6 program[29] with the aid of the program WinGX.[30] H atoms bonded to C were generated stereochemically and refined by the riding model. After having placed C-bound H atoms, those bonded to O and N, that are essential in the identification of tautomers, were clearly found in difference Fourier maps as the first maxima and their coordinates were refined with some restraints on bond length. For all H atoms U_{iso} was set at 1.2 times U_{eq} of the carrier atom (1.5 in the case of methyl group). The analysis of the crystal packing was performed using the program Mercury.[31] CCDC 1857839−1857846 contain the supplementary crystallographic data for this article.

TT6·HCl·H_2O: $C_{10}H_{12}ClN_5O_2$, M_r = 269.70, triclinic, $P\bar{1}$, Z = 2, colorless, a = 5.7230(10) Å, b = 7.365(2) Å, c = 13.889(4) Å, α = 88.539(10)°, β = 88.740(10)°, γ = 82.39(2)°, V = 580.0(3) Å^3, T = 293 K, 4809 reflns collected, 2605 unique (R_{int} = 0.0231), R = 0.0418 ($I > 2\sigma(I)$), wR (all) = 0.1164, GOF = 1.066, final max/min peak 0.243/−0.230 e/Å^3. CCDC 1857839.

2[TT6·HBr]·3H_2O: $C_{20}H_{26}Br_2N_{10}O_5$, M_r = 646.32, monoclinic, $C2/c$, Z = 4, colorless, a = 23.746(7) Å, b = 6.751(3) Å, c = 16.917(5) Å, α = 90°, β = 102.32(2)°, γ = 90°, V = 2649.5(16) Å^3, T = 293 K, 12724 reflns collected, 2965 unique (R_{int} = 0.0374), R = 0.0470 ($I > 2\sigma(I)$), wR (all) = 0.1047, GOF = 1.115, final max/min peak 0.611/−0.391 e/Å^3. CCDC 1857840.

TT6·$HClO_4$: $C_{10}H_{10}ClN_5O_5$, M_r = 315.68, monoclinic, $C2/m$, Z = 4, colorless, a = 13.107(5) Å, b = 7.004(3) Å, c = 13.851(6) Å, α = 90°, β = 100.36(2)°, γ = 90°, V = 1250.8(9) Å^3, T = 293 K, 6522 reflns collected, 1547 unique (R_{int} = 0.0403), R = 0.0416 ($I > 2\sigma(I)$), wR (all) = 0.1049, GOF = 1.045, final max/min peak 0.311/−0.400 e/Å^3. CCDC 1857841.

(TT6H)(HSO_4): $C_{10}H_{11}N_5O_5S$, M_r = 313.30, monoclinic, $C2/c$, Z = 8, colorless, a = 17.195(5) Å, b = 6.242(3) Å, c = 24.702(6) Å, α = 90°, β = 107.03(3)°, γ = 90°, V = 2535.1(16) Å^3, T = 293 K, 4992 reflns collected, 2764 unique (R_{int} = 0.0243), R = 0.0414 ($I > 2\sigma(I)$), wR (all) = 0.1116, GOF = 1.057, final max/min peak 0.240/−0.367 e/Å^3. CCDC 1857842.

DOI: 10.1021/acs.cgd.8b01158
Cryst. Growth Des. XXXX, XXX, XXX−XXX

2[(TT6H)(HSO$_4$)]·(TT6H)$_2$SO$_4$·4H$_2$O: $C_{40}H_{50}N_{20}O_{20}S_3$, M_r = 1227.18, triclinic, $P\bar{1}$, Z = 2, colorless, a = 12.997(3) Å, b = 14.596(4) Å, c = 14.977(7) Å, α = 77.73(7)°, β = 78.870(13)°, γ = 64.30(8)°, V = 2485(2) Å^3, T = 173 K, 42899 reflns collected, 10903 unique (R_{int} = 0.0632), R = 0.0562 ($I > 2\sigma(I)$), wR(all) = 0.1395, GOF = 1.062, final max/min peak 0.575/−0.640 e/Å^3. CCDC 1857843.

TT7·HCl: $C_{10}H_{10}ClN_5O$, M_r = 251.68, monoclinic, $P2_1/c$, Z = 4, colorless, a = 7.044(3) Å, b = 8.934(4) Å, c = 18.301(7) Å, α = 90°, β = 105.253(10)°, γ = 90°, V = 1111.1(8) Å^3, T = 293 K, 6662 reflns collected, 2458 unique (R_{int} = 0.0790), R = 0.0593 ($I > 2\sigma(I)$), wR (all) = 0.1303, GOF = 1.033, final max/min peak 0.284/−0.340 e/Å^3. CCDC 1857844.

TT7·HBr·3H$_2$O: $C_{10}H_{16}BrN_5O_4$, M_r = 350.19, triclinic, $P\bar{1}$, Z = 2, colorless, a = 6.7830(12) Å, b = 9.6050(15) Å, c = 12.7370(11) Å, α = 106.651(9)°, β = 96.355(10)°, γ = 102.920(11)°, V = 761.2(2) Å^3, T = 293 K, 8939 reflns collected, 3407 unique (R_{int} = 0.0393), R = 0.0503 ($I > 2\sigma(I)$), wR (all) = 0.1252, GOF = 1.082, final max./min peak 0.479/-0.482 e/Å^3. CCDC 1857845.

2[TT7·HClO$_4$]·H$_2$O: $C_{20}H_{12}Cl_2N_{10}O_{11}$, M_r = 649.38, triclinic, $P\bar{1}$, Z = 2, colorless, a = 8.0260(5) Å, b = 13.3910(13) Å, c = 13.8430(10) Å, α = 112.786(7)°, β = 100.887(7)°, γ = 96.787(7)°, V = 1316.57(19) Å^3, T = 293 K, 22073 reflns collected, 5988 unique (R_{int} = 0.0316), R = 0.0459 ($I > 2\sigma(I)$), wR(all) = 0.1283, GOF = 1.055, final max./min peak 0.647/−0.353 e/Å^3. CCDC 1857846.

Computational Details. Quantum chemical computations were carried with the Gaussian 09 package by using density functional theory (DFT).[32] The BMK meta functional[33] was employed throughout in conjunction with the 6-31+G** basis set. Owing to its high fraction (42%) of HF exchange which mitigates the self-interaction problem,[34] BMK has proven to give excellent performance, nearly reproducing experimental electrical and optical properties for donor−acceptor systems,[35] matching the quality of highly parametrized functionals, correlated post-Hartee-Fock and ad hoc parametrized methods.[36−39] Solvent (water) effects were included by the polarizable continuum model (PCM).[40] Starting geometries of the dimeric patterns reported in Chart 6 were generated in planar configuration. Optimized structures for single molecules and hydrogen-bonded dimers were obtained by DFT computations carried out without imposing any geometrical constraint. The nature of located stationary points was verified by checking the eigenvalues of the Hessian matrix; all the minimum energy structures have positive eigenvalues.

CONCLUSIONS

Within the class of 4-methyl-7-hydroxyphenyl-[1,2,4]triazolo-[3,2-*c*][1,2,4]triazoles, the placement of the OH group in different positions on the phenyl ring (ortho, meta, para) has an effect on the energy of the single different tautomer molecules. However, we have shown that it also affects the energy of the modes of pairing of the different tautomer molecules via strong hydrogen bonding, and hence the selective crystallization of the tautomeric forms. A particularly striking evidence of the latter issue is observed, for the monoprotonated triazolo-triazolium cations, in the case of the para and meta positions. In fact, even if the energy difference of the tautomers 1H-3H and 2*H*-3*H* is small for singly protonated TT5 (para OH) and even smaller for singly protonated TT6 (meta OH), the outcome of the crystallization experiments is completely different: only 2*H*-3*H* for TT6, independent of the counterion, either 1*H*-3*H* or 2*H*-3*H* for TT5 depending on the counterion.

ASSOCIATED CONTENT

Supporting Information

The Supporting Information is available free of charge on the ACS Publications website at DOI: 10.1021/acs.cgd.8b01158.

Detailed synthetic procedures, including ^{1}H NMR, ^{13}C NMR and mass spectra of final compounds and intermediates; detailed description of the UV−vis and electrochemical methods used in the study of acid−base properties; geometry of DFT optimized H-bonded dimers; tables of H-bonding distances from single crystal X-ray analysis; full packing diagrams. Observed and calculated UV−vis spectrum of TT6 at very acidic pH (PDF)

Accession Codes

CCDC 1857839−1857846 contain the supplementary crystallographic data for this paper. These data can be obtained free of charge via www.ccdc.cam.ac.uk/data_request/cif, or by emailing data_request@ccdc.cam.ac.uk, or by contacting The Cambridge Crystallographic Data Centre, 12 Union Road, Cambridge CB2 1EZ, UK; fax: +44 1223 336033.

AUTHOR INFORMATION

Corresponding Authors

*(S.F.) E-mail: sandra.fusco@unina.it.
*(A.C.) E-mail: acapobianco@unisa.it.
*(R.C.) E-mail: roberto.centore@unina.it.

ORCID

Amedeo Capobianco: 0000-0002-5157-9644
Andrea Peluso: 0000-0002-6140-9825
Fabio Borbone: 0000-0001-7433-9267
Roberto Centore: 0000-0002-2797-0117

Notes

The authors declare no competing financial interest.

ACKNOWLEDGMENTS

Thanks are due to COST association for support and critical discussions within the COST Action CM-1402-Crystallize and to the CRdC NTAP of Regione Campania (Italy) for the X-ray facility.

REFERENCES

(1) Entry "tautomerism" in *IUPAC, Compendium of Chemical Terminology*, 2nd ed. (the "Gold Book"); Compiled by McNaught, A. D.; Wilkinson, A., Blackwell Scientific Publications: Oxford, 1997.
(2) Watson, J. D.; Crick, F. H. C. Genetical implications of the structure of deoxyribonucleic acid. *Nature* **1953**, *171*, 964−967.
(3) Goodman, M. F. Mutations caught in the act. *Nature* **1995**, *378*, 237−238.
(4) Wang, W.; Hellinga, H. W.; Beese, L. S. Structural evidence for the rare tautomer hypothesis of spontaneous mutagenesis. *Proc. Natl. Acad. Sci. U. S. A.* **2011**, *108*, 17644−17648.
(5) Martin, Y. C. Let's not forget tautomers. *J. Comput.-Aided Mol. Des.* **2009**, *23*, 693−704.
(6) Desiraju, G. R. Intramolecular Proton Transfers in the Solid State. Conversion of the Hydroxyazo into the Quinone Hydrazone Tautomer of 2-Amino-3-hydroxy-6-phenylazopyridine. X-Ray Crystal Structures of the Two Forms. *J. Chem. Soc., Perkin Trans. 2* **1983**, 1025−1030.
(7) Hanus, M.; Ryjáček, F.; Kabeláč, M.; Kubař, T.; Bogdan, T. V.; Trygubenko, S. A.; Hobza, P. Correlated ab Initio Study of Nucleic Acid Bases and Their Tautomers in the Gas Phase, in a Microhydrated Environment and in Aqueous Solution. Guanine: Surprising Stabilization of Rare Tautomers in Aqueous Solution. *J. Am. Chem. Soc.* **2003**, *125*, 7678−7688.
(8) Zhang, C.; Xie, L.; Ding, Y.; Sun, Q.; Xu, W. Real-Space Evidence of Rare Guanine Tautomer Induced by Water. *ACS Nano* **2016**, *10*, 3776−3782.

DOI: 10.1021/acs.cgd.8b01158
Cryst. Growth Des. XXXX, XXX, XXX−XXX

(9) Marshall, M. G.; Lopez-Diaz, V.; Hudson, B. S. Single-Crystal X-ray Diffraction Structure of the Stable Enol Tautomer Polymorph of Barbituric Acid at 224 and 95 K. *Angew. Chem., Int. Ed.* **2016**, *55*, 1309−1312.
(10) Ladenthin, J. N.; Frederiksen, T.; Persson, M.; Sharp, J. C.; Gawinkowski, S.; Waluk, J.; Kumagai, T. Force-induced tautomerization in a single molecule. *Nat. Chem.* **2016**, *8*, 935−940.
(11) Bussetti, G.; Campione, M.; Riva, M.; Picone, A.; Raimondo, L.; Ferraro, L.; Hogan, C.; Palummo, M.; Brambilla, A.; Finazzi, M.; Duò, L.; Sassella, A.; Ciccacci, F. Stable Alignment of Tautomers at Room Temperature in Porphyrin 2D Layers. *Adv. Funct. Mater.* **2014**, *24*, 958−963.
(12) Horiuchi, S.; Kobayashi, K.; Kumai, R.; Ishibashi, S. Proton tautomerism for strong polarization switching. *Nat. Commun.* **2017**, *8*, 14426.
(13) Cruz-Cabeza, A. J.; Groom, C. R. Identification, classification and relative stability of tautomers in the cambridge structural database. *CrystEngComm* **2011**, *13*, 93−98.
(14) Allen, F. H. The Cambridge Structural Database: a quarter of a million crystal structures and rising. *Acta Crystallogr., Sect. B: Struct. Sci.* **2002**, *58*, 380−388.
(15) Centore, R.; Concilio, S.; Panunzi, B.; Sirigu, A.; Tirelli, N. Nonlinear Optical Properties of Some Side Chain Copolymers Based on Benzoxazole Containing Chromophores. *J. Polym. Sci., Part A: Polym. Chem.* **1999**, *37*, 603−608.
(16) Carella, A.; Centore, R.; Mager, L.; Barsella, A.; Fort, A. Crosslinkable organic glasses with quadratic nonlinear optical activity. *Org. Electron.* **2007**, *8*, 57−62.
(17) Fusco, S.; Centore, R.; Riccio, P.; Quatela, A.; Stracci, G.; Archetti, G.; Kuball, H.-G. NLO-active polymers containing triazolo-thiadiazole segments. *Polymer* **2008**, *49*, 186−191.
(18) Centore, R.; Fusco, S.; Capobianco, A.; Piccialli, V.; Zaccaria, S.; Peluso, A. Tautomerism in the Fused N-Rich Triazolotriazole Heterocyclic System. *Eur. J. Org. Chem.* **2013**, *2013*, 3721−3728.
(19) Centore, R.; Manfredi, C.; Fusco, S.; Maglione, C.; Carella, A.; Capobianco, A.; Peluso, A.; Colonna, D.; Di Carlo, A. Proton induced tautomeric switching in N-rich aromatics with tunable acid-base character. *J. Mol. Struct.* **2015**, *1093*, 119−124.
(20) Centore, R.; Manfredi, C.; Capobianco, A.; Volino, S.; Ferrara, M. V.; Carella, A.; Fusco, S.; Peluso, A. Solid State Separation and Isolation of Tautomers of Fused-Ring Triazolotriazoles. *J. Org. Chem.* **2017**, *82*, 5155−5161.
(21) Allen, F. H.; Motherwell, W. D. S.; Raithby, P. R.; Shields, G. P.; Taylor, R. Systematic analysis of the probabilities of formation of bimolecular hydrogen-bonded ring motifs in organic crystal structures. *New J. Chem.* **1999**, *23*, 25−34.
(22) Cruz-Cabeza, A. J.; Reutzel-Edens, S. M.; Bernstein, J. Facts and fictions about polymorphism. *Chem. Soc. Rev.* **2015**, *44*, 8619−8635.
(23) Davey, R. J.; Allen, K.; Blagden, N.; Cross, W. I.; Lieberman, H. F.; Quayle, M. J.; Righini, S.; Seton, L.; Tiddy, G. J. T. Crystal engineering − nucleation, the key step. *CrystEngComm* **2002**, *4*, 257−264.
(24) Causà, M.; Centore, R. Actual and virtual structures in molecular crystals. *CrystEngComm* **2017**, *19*, 1320−1327.
(25) Centore, R.; Carella, A.; Fusco, S. Supramolecular synthons in fluorinated and nitrogen-rich *ortho*-diaminotriazoles. *Struct. Chem.* **2011**, *22*, 1095−1103.
(26) Gans, P.; Sabatini, A.; Vacca, A. Investigation of equilibria in solution. Determination of equilibrium constants with the *HYPERQUAD* suite programs. *Talanta* **1996**, *43*, 1739−1753.
(27) *SADABS*; Bruker-Nonius: Delft, The Netherlands, 2002.
(28) Altomare, A.; Burla, M. C.; Camalli, M.; Cascarano, G. L.; Giacovazzo, C.; Guagliardi, A.; Moliterni, G. G.; Polidori, G.; Spagna, R. *SIR97*: a new tool for crystal structure determination and refinement. *J. Appl. Crystallogr.* **1999**, *32*, 115−119.
(29) Sheldrick, G. M. Crystal structure refinement with. *Acta Crystallogr., Sect. C: Struct. Chem.* **2015**, *71*, 3−8.
(30) Farrugia, L. J. *WinGX* and *Ortep for Windows*: an update. *J. Appl. Crystallogr.* **2012**, *45*, 849−854.
(31) Macrae, C. F.; Bruno, I. J.; Chisholm, J. A.; Edgington, P. R.; McCabe, P.; Pidcock, E.; Rodriguez-Monge, L.; Taylor, R.; van de Streek, J.; Wood, P. A. *Mercury CSD 2.0* − new features for the visualization and investigation of crystal structures. *J. Appl. Crystallogr.* **2008**, *41*, 466−470.
(32) Frisch, M. J.; Trucks, G. W.; Schlegel, H. B.; Scuseria, G. E.; Robb, M. A.; Cheeseman, J. R.; Scalmani, G.; Barone, V.; Mennucci, B.; Petersson, G. A.; Nakatsuji, H.; Caricato, M.; Li, X.; Hratchian, H. P.; Izmaylov, A. F.; Bloino, J.; Zheng, G.; Sonnenberg, J. L.; Hada, M.; Ehara, M.; Toyota, K.; Fukuda, R.; Hasegawa, J.; Ishida, M.; Nakajima, T.; Honda, Y.; Kitao, O.; Nakai, H.; Vreven, T.; Montgomery, J. A., Jr.; Peralta, J. E.; Ogliaro, F.; Bearpark, M.; Heyd, J. J.; Brothers, E.; Kudin, K. N.; Staroverov, V. N.; Kobayashi, R.; Normand, J.; Raghavachari, K.; Rendell, A.; Burant, J. C.; Iyengar, S. S.; Tomasi, J.; Cossi, M.; Rega, N.; Millam, J. M.; Klene, M.; Knox, J. E.; Cross, J. B.; Bakken, V.; Adamo, C.; Jaramillo, J.; Gomperts, R.; Stratmann, R. E.; Yazyev, O.; Austin, A. J.; Cammi, R.; Pomelli, C.; Ochterski, J. W.; Martin, R. L.; Morokuma, K.; Zakrzewski, V. G.; Voth, G. A.; Salvador, P.; Dannenberg, J. J.; Dapprich, S.; Daniels, A. D.; Farkas, O.; Foresman, J. B.; Ortiz, J. V.; Cioslowski, J.; Fox, D. J., *Gaussian 09*, Revision A02; Gaussian Inc.: Wallingford, CT, 2009.
(33) Boese, A. D.; Martin, J. M. L. Development of Density Functionals for Thermochemical Kinetics. *J. Chem. Phys.* **2004**, *121*, 3405−3416.
(34) Peach, M. J. G.; Benfield, P.; Helgaker, T.; Tozer, D. J. Excitation Energies in Density Functional Theory: An Evaluation and a Diagnostic Test. *J. Chem. Phys.* **2008**, *128*, 044118−8.
(35) Capobianco, A.; Centore, R.; Noce, C.; Peluso, A. Molecular hyperpolarizabilities of push−pull chromophores: A comparison between theoretical and experimental results. *Chem. Phys.* **2013**, *411*, 11−16.
(36) Suponitsky, K. Y.; Tafur, S.; Masunov, A. E. Applicability of Hybrid Density Functional Theory Methods to Calculation of Molecular Hyperpolarizability. *J. Chem. Phys.* **2008**, *129*, 044109−15.
(37) Capobianco, A.; Centore, R.; Fusco, S.; Peluso, A. Electro-optical properties from CC2 Calculations: A comparison between theoretical and experimental results. *Chem. Phys. Lett.* **2013**, *580*, 126−129.
(38) Castaldo, A.; Centore, R.; Peluso, A.; Sirigu, A.; Tuzi, A. Structure and Electronic Properties of Extended Chromophores for Applications in Second-Order Nonlinear Optics. *Struct. Chem.* **2002**, *13*, 27−36.
(39) Capobianco, A.; Esposito, A.; Caruso, T.; Borbone, F.; Carella, A.; Centore, R.; Peluso, A. Tuning Wavefunction Mixing in Push−Pull Molecules: From Neutral to Zwitterionic Compounds. *Eur. J. Org. Chem.* **2012**, *2012*, 2980−2989.
(40) Miertuš, S.; Scrocco, E.; Tomasi, J. Electrostatic Interaction of a Solute with a Continuum. A Direct Utilization of Ab Initio Molecular Potentials for the Prevision of Solvent Effects. *Chem. Phys.* **1981**, *55*, 117−129.

DOI: 10.1021/acs.cgd.8b01158
Cryst. Growth Des. XXXX, XXX, XXX−XXX